Anbar Journal of Engineering Science (AJES)
P-ISSN: 1997-9428; E-ISSN: 2705-7440

Vol. 12 , No. 1 (2021) , pp. 47 ~ 56
DOI: 10.37649/aengs.2021.171197

University of Anbar

Anbar Journal of Engineering Science©

journal homepage: http:// www.uoanbar.edu.iq/Evaluate/

Effect of Anchorage Length on the Shear Capacity of High Strength Concrete Deep Beams

Maytham Khalid Gatea [a], ***Dr. David A.M.Jawad*** [b]

[a] ***Department of Civil Engineering, College of Engineering, University of Basrah, Al-Basrah, 61004, Iraq*** *(PhD candidate University of Basrah)*
[b] ***Department of Civil Engineering, College of Engineering, University of Basrah, Al-Basrah, 61004, Iraq*** *(Asst. Professor University of Basrah)*

PAPER INFO

Paper history:
Received 18/1/2021
Revised 27/2/2021
Accepted 08/3/2021

Keywords:
Anchorage Length, Shear Capacity, High Strength Concrete, Deep Beam.

ABSTRACT

Ten simply supported deep beams with high strength concrete (C55 MPa) have been casted and subjected to a four-point loading test. Different parameters were examined for their influence on specimen behavior. These parameters were the shear span to overall depth ratio (a/h), the overall depth of deep beams (h), and additional anchorage length beyond the centerline of support (la). The experimental results show that the beam capacity decreases as the shear span to the overall depth ratio increases, and the overall depth and embedment length decrease. The major effect of anchorage length on the shear strength is studied. Different failure modes were observed which do not match strut-and-tie failure modes. The shear compression and anchorage failures were controlled in the high compressive concrete deep beams due to bottom steel yielding. Finally, the experimental test results are compared with predictions of the strut-and-tie method according to the ACI 318-14 and a good agreement was found.

1. Introduction

The reinforced concrete deep beam is a structural member recognized by having a larger beam section compared to its span for which a significant portion of the load is transferred by a single strut directly to the support [1]. AC1 318-14 defines a beam as a deep beam when the clear span does not exceed four times the overall depth of member (h), or a shear span does not exceed twice the overall depth of the member [2]. The structural deep beam is used in many engineering applications such as the shear walls, floor diaphragms, foundation pile-caps, and offshore gravity type structures [3]. Due to deep beam geometric proportions, the shear generally controls the RC deep beam capacity, instead of flexure, so the shear capacity is very important in design [1]. The dividing line between normal-strength and high-strength concrete is 55 MPa as classified by ACI 363.2R-11 [4]. Steel reinforcement plays an essential role in resisting tensile stresses in a concrete structure. Proper detailing of the anchorage regions, particularly at supports is also essential. Anchorage can be provided in several ways by providing hooks, straight bar embedment length, headed bars, or any other mechanical anchorage [5]. The structural mechanics of the bond between concrete and deformed reinforcing bar consists of three essential components: the surface friction between the concrete and steel bar, the mechanical interaction of concrete against the bar deformation, and the chemical adhesion [6]. Slippage of steel reinforcement in concrete may occur if the bar is stressed up to the cutoff point. This takes place when the embedment length of the bar is not sufficiently long. The extension of steel reinforcement is a result of the accumulation of strains along the length of the bar. The combined effect of reinforcement extension and slip in the adjoining member may be referred to as an anchorage slip [7]. Azizinamini, A. et al. were concluded that in the case of high-strength concrete (HSC), increasing the tension development length (or equivalently tension splices) is not an efficient way of increasing the bond capacity of deformed reinforcing bars, especially when the cover concrete is small [8]. The size of the bearing plates may affect the principal stresses significantly and is

* Corresponding author. :Maytham Khalid Gatea: maythan890@gmail.com ; +964 7724561289

very critical in the immediate vicinity of supports and the anchorage conditions of the tensile reinforcement is another important aspect for the design of deep beams [9]. Perry A. and Zongyu Z. found that when compression struts are confined by plain concrete, the maximum bearing stress to cause transverse splitting depends on the amount of confinement, as well as the aspect ratio (height/width) of the compression strut. The concrete bearing strength is proportional to the concrete tensile strength [10].

A few deep beam studies investigated the influence of the anchorage effect on the behavior of RC deep beams. Sung-Gul Hong, et al. tested eight rectangular simply support deep beams with normal concrete to study the shear strength combined with end anchorage failure [11]. Fung-Kew Kong et al. also studied the embedding length of main tension steel in normal strength lightweight concrete deep beams [12]. This study is made to present failure mechanisms for determining the ultimate strength of reinforced concrete deep beams related to end anchorage failure for high strength concrete deep beam.

2. Experimental program

The experimental work and the conducted tests were carried out in the laboratories of the college of engineering at Basra University.

2.1 Materials

The raw materials of concrete are cement, coarse aggregates (gravel), fine aggregates (sand), and mixed with water which hardens with time. Deformed bars (Grade 60) were used.

1. Cement

Ordinary portland cement (type I) was used in the mix design of concrete to cast all specimens throughout this program. The physical properties and chemical compositions of selected cement comply with ASTM C150[13].

2. Coarse Aggregate

Crushed gravel was provided from Jabal Sanam at Basra province to be used as a coarse aggregate in this study. The sieve analysis of coarse aggregate was according to ASTM C136 [14] and complied with ASTM C33[15].

3. Fine Aggregate

Natural sand from Jabal Sanam at Al Zubair city was provided for use in concrete mixes of this research scope. The sieve analysis result was carried out according to ASTM C 136 [14]. The obtained sieve analysis results indicated that the fine aggregate grading was within the ASTM C 33 [15] limits requirements.

4. Water

Potable water meeting the requirements of ASTM C1602 [16] was used for mixing, casting as well as curing of concrete.

5. Superplasticizer (SP)

Sika ViscoCrete F180G that complies with ASTM C494 [17] (Type F & G) and C1017 [18] (Type I & II) was used throughout this work as a high-performance superplasticizer. It is a high range water reducer that provides long workability times, high density, and high strength. The nominal dosage of Sika ViscoCrete F180G is (500 –1000 g for 100 kg cement) as recommended by the manufacturer datasheet.

6. Steel Reinforcement

Grade 60 Ukrainian steel bars with protrusions (deformed bars) were used in this research. Ø 12 mm and Ø 20 mm were utilized for top and bottom longitudinal reinforcement respectively, and Ø 10 mm were used for stirrups. Three samples from each bar with the same diameter and manufacturer's heat number were tested by testing machines available in the laboratory of the Mechanical Department at Basra University. Mechanical test results are shown in Table 1, which was carried out according to ASTM A 615 [19].

Table 1. Properties of Reinforcing Bars

Bar size (mm)	Test results		
	Yield stress (N/mm2)	Ultimate Strength (N/mm2)	Elongation (%)
10	440	643	12
16	480	660	12
20	530	680	10

2.2 Concrete Mix Design

High strength concrete with C 55 MPa cylinder compressive strength value at the age of 28 days was used to pour the studied deep beams with different parameters. Concrete raw materials were natural sand, crushed gravel, portland cement, and water with a superplasticizer. The water to cement ratio has been reduced to produce high strength concrete and a suitable quantity of superplasticizer was used to get good workability. The mix proportions by weight were 1:1.1:2.2 (cement: gravel: sand). Table 2 shows the mix designation and amount of used mixed materials.

Table 2. HCS Mix Design

Materials	**Quantity/m^3**

Water (*l*)	159
Cement (kg)	530
Sand (kg)	583
Gravel (kg)	1166
Superplasticizer	0.7%

1. *Beams details*

The experimental program consists of casting and testing ten reinforced concrete deep beams. Four different shear span to overall depth ratio (a/h), the overall depth (h), and embedment length beyond the support (la) were studied as presented in Fig 1. and Tables 3, 4, and 5.

Table 3. Shear span to depth ratio parameter

Designation	a (mm)	H (mm)	a/h
Control Beam	450	300	1.50
DB2-a	375	300	1.25
DB3-a	300	300	1.00
DB4-a	225	300	0.75

Table 4. The overall depth parameter

Designation	H (mm)	a (mm)
Control Beam	300	450
DB2-H	360	450
DB3-H	400	450
DB4-H	450	450

Table 5. The embedment length beyond the support parameter

Designation	l_a (mm)	H (mm)	a (mm)
Control Beam	150	300	450
DB2-l_a	100	300	450
DB3-l_a	50	300	450
DB4-l_a	0	300	450

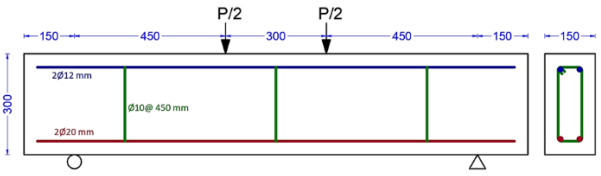

Control Beam Detail

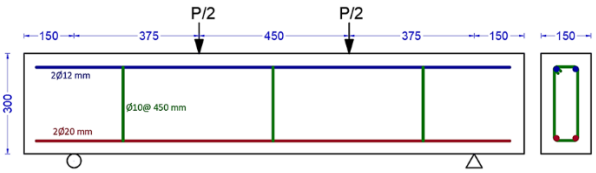

DB2-a Detail

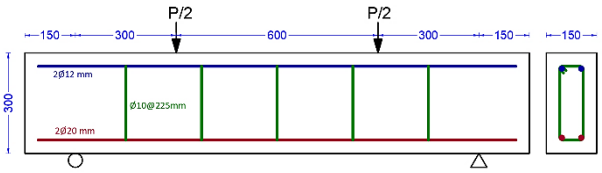

DB3-a Detail

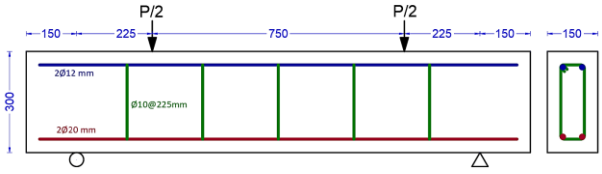

DB4-a Detail

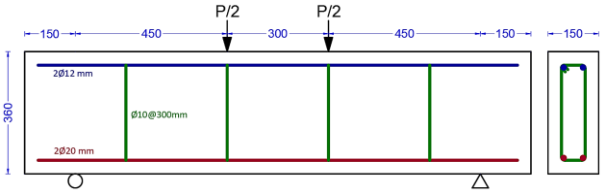

DB2-H Detail

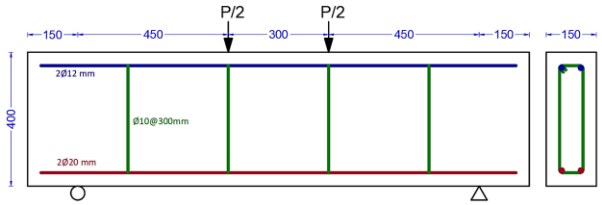

DB3-H Detail

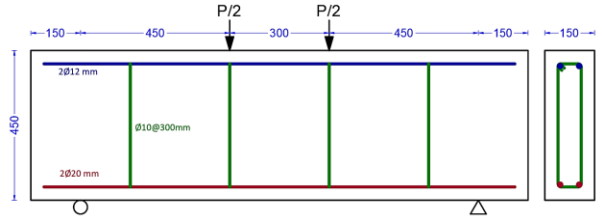

DB4-H Detail

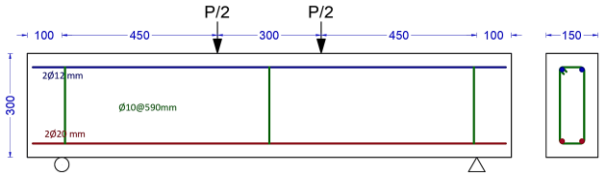

DB2-l_a Detail

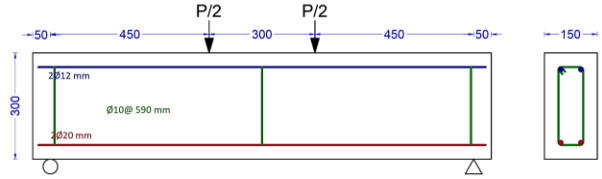

DB3-l_a Detail

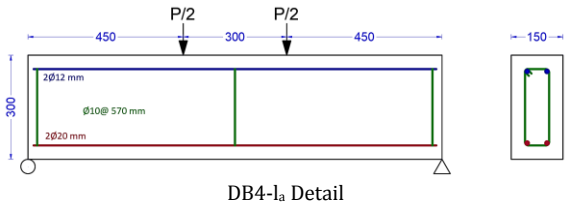

DB4-l_a Detail

Figure 1. Details of deep beam specimens

3. Specimens Pouring Procedure

Specimens pouring procedure is divided into three stages as follows:

1. Pre-pouring stage
2. Pouring stage
3. Post-pouring stage

18 mm thick plywood with horizontal and vertical shuttering / supports was utilized for the fabrication of the wood molds to support the green concrete of casted specimens. A tilting drum mixer of the concrete laboratory was used to produce fresh concrete by mixing water, cement, aggregates, and admixtures. After the mixing process was completed, the slump test and temperature measurement were conducted in accordance with ACI 301 [20]. A set of nine cylinders and cubes for each group batching were taken for concrete compressive, splitting, and modulus of elasticity tests. Plastic sheets were applied to concrete surfaces immediately after the casting finishing to prevent water evaporation. The final curing measure was applied after the bleed water shine disappeared, and the concrete reached the final set by covering with saturated burlap to prevent water loss as well as supplying additional curing water to sustain cement hydration.

3.1 Test Procedure

All specimens were simply supported and loaded at two points. Fig 2 shows the typical beam set up prior to the test. Different stiff steel spreader beams were used to distribute the load from the crosshead of the universal testing machine to the two loading points. Steel plates with 250 mm length, 100 mm width, and 50 mm thickness were used as bearing plates at the load points and supports.

White color was used to paint all beam specimens two days prior to testing to identify the resulting cracks during the loading stage. The ultimate load was applied through the two loading points incrementally. The mid-span deflection and corresponding applied load were taken each 10 kN. A digital dial gauge was used to measure the mid-span deflection as shown in Fig 3. All cracks were marked with a black marker and the crack widths were measured using a digital reading instrument as shown in Fig 4.

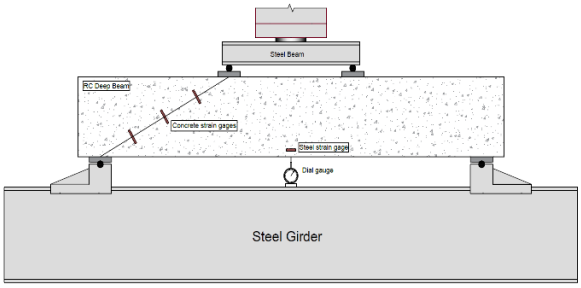

Figure 2. General set up.

Figure 3. Digital dial gauge.

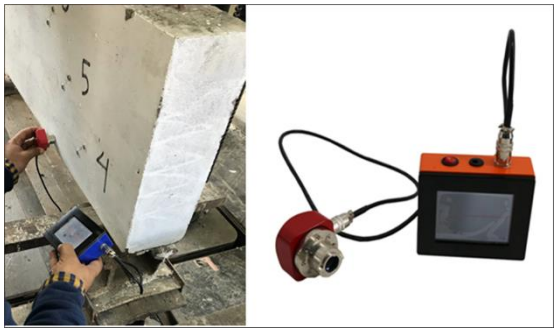

Figure 4. Digital Concrete Crack Width Gauge Tester.

4. Results and Discussion

The first diagonal cracking load (PScr), the first hairline flexural cracking load (PFcr), and the ultimate load (Pu), and the load-deflection response, crack propagation are indicated in this study. Each specimen was studied based on the information obtained from manual readings, photographs, and data acquisition systems.

4.1 First Diagonal Cracking, Flexural Cracking, and Ultimate Loads

The effect of shear span to overall depth, overall depth, and embedment length on the beam capacity was presented in Figs 5 to 7 and Table 6. The obtained results confirm that the behavior of reinforced concrete deep beams is dominated by the shear span to depth ratio and the ultimate load capacity decreases with the increase in the shear span to depth ratio as shown in Fig 5. Generally, increasing the depth of the beam leads to an increase in the load-

carrying capacity as noted in Fig 6. It is also observed that progressive reductions of the additional embedment length beyond the support, yields to proportional reductions in the ultimate loads due to the reduction of the bond strength after nodal zones, as shown in Fig 7.

Table 6. First Flexural Cracking, Diagonal, and Ultimate Loads

Designation	P_u (kN)	P_{Scr} (kN)	P_{Fcr} (kN)
Control Beam	390	70	160
DB2-a	420	80	180
DB3-a	510	80	250
DB4-a	650	120	260
DB2-H	480	100	240
DB3-H	520	120	250
DB4-H	560	140	230
DB2-l_a	375	70	150
DB3-l_a	325	60	120
DB4-l_a	300	50	100

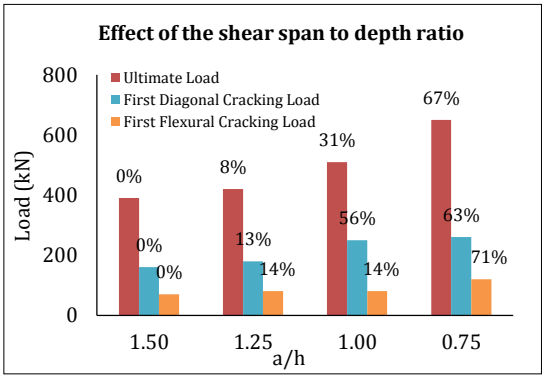

Figure 5. Effect of (a/h) on the beam capacity.

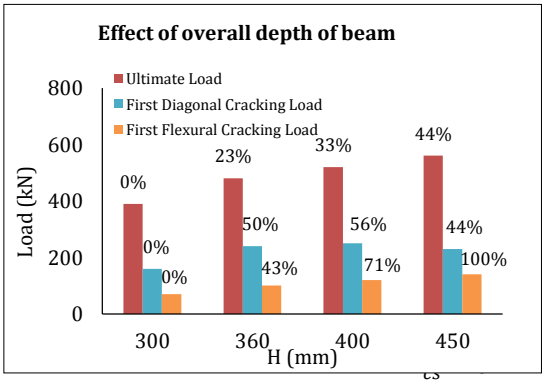

Figure 6. Effect of (h) on the beam capacity.

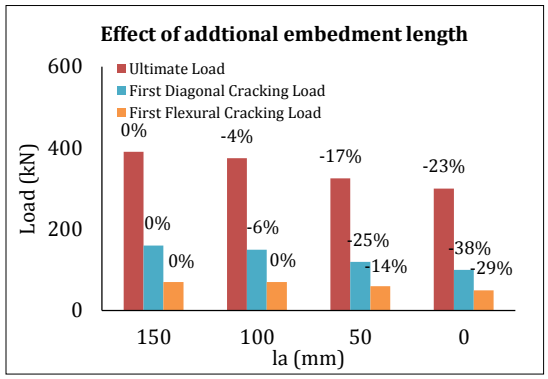

Figure 7. Effect of (la) on the beam capacity.

The strut-and-tie method (STM)-ACI 318 -14 is used for predicting the ultimate capacity and the failure modes of the reinforced concrete deep beams [2]. The flow of internal forces in the deep beam is idealized as a truss carrying the imposed loading through the region to its supports as shown in Fig 8. Three main components must be checked according to the strut-and-tie method:

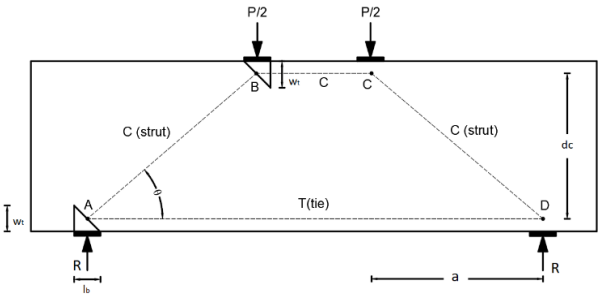

Figure 8. Internal forces flow in the deep beam.

1-Strength of struts

No longitudinal reinforcement crosses the strut path in this study, so the nominal compressive strength of a strut was calculated by:

$\times A_{cs}$

$\times f_c'$

$\times w_s$ (3)

$$w_s = w_t \times \sin\theta_s + l_p$$

$\times \cos\theta_s$ (4)

$\leq 25°$

2-Strength of ties

For evaluation of the strength of ties for non-restressed members, F_{nt}, ACI 318 proposes:

$$F_{ns} = f_y \times A_{ts} \quad (6)$$

3-Strength of nodal zones

The nominal compression strength of a nodal zone, F_{nn}, is proposed as following:

$$F_{ns} = f_{ce} \times A_{nz} \quad (7)$$

$$f_{ce} = 0.85\,\beta_n \times f_c' \quad (8)$$

The lowest strength value of strut, tie, and the nodal zone is selected as the failure load as recommended by the strut-and-tie method.

The ultimate loads capacity and the failure modes are summarized in Table 7. A comparison between the results of the strut-and-tie method and the experimental values of the ultimate load for the effect of the shear span to depth ratio, the overall depth, and additional embedment length beyond the support are shown in Figs 9, 10, and 11.

Table 7. The ultimate load values and failure modes predicted by STM.

Designation	P_u (kN) EXP	P_u (kN) STM	Failure Mode
Control Beam	390	328	Tie
DB2-a	420	394	Tie
DB3-a	510	493	Tie
DB4-a	650	657	Tie
DB2-H	480	422	Tie
DB3-H	520	485	Tie
DB4-H	560	563	Tie
DB2-l_a	375	328	Tie
DB3-l_a	325	328	Tie
DB4-l_a	300	328	Tie

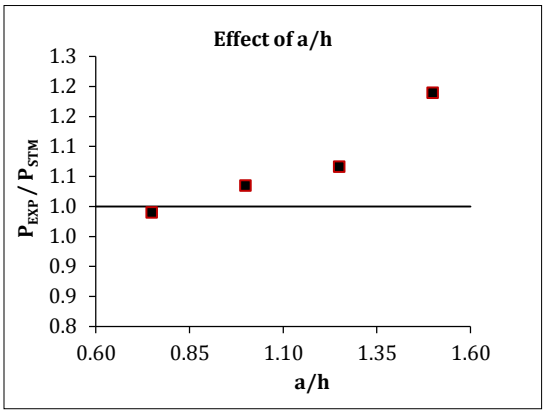

Figure 9. Comparison of code predictions to test results (effect of a/h).

According to Fig 9, the results show that ACI 318-14 has a good agreement and generally conservative for specimens with different a/h ratio.

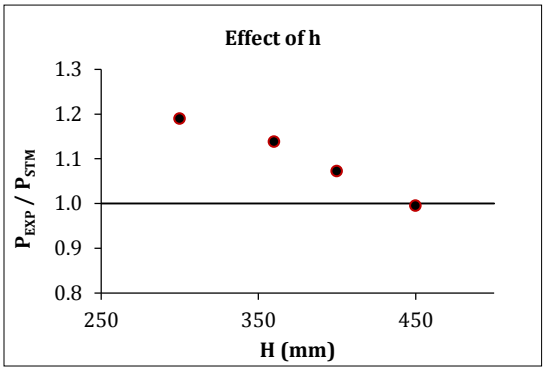

Figure 10. Comparison of code predictions to test results (effect of h).

The implementation of STM can predict the ultimate load capacity of deep beams with a good degree of accuracy compared with experimental results as shown in Fig 10.

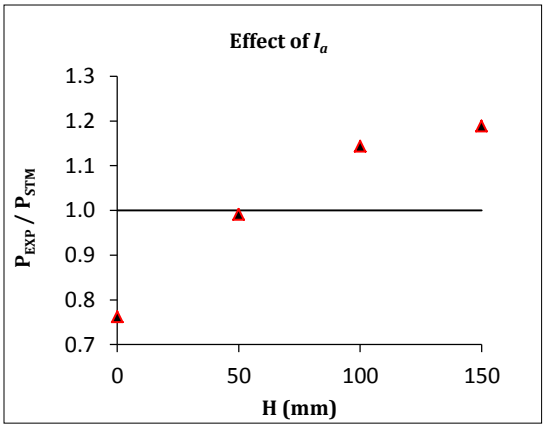

Figure 11. Comparison of code predictions to test results (effect of La)

On the other hand, a comparison between the ex-

perimental and predicted ultimate load capacity according to ACI 318-14 is shown in Fig 11 as a function of additional embedment length beyond the support. The STM approach does not account for the effect of different additional embedded lengths beyond the support on the ultimate strength and failure mode. Therefore, the predicted failure modes by STM were different from those found experimentally, especially for the beam with la less than 50 mm. A clear deviation has been observed in these results due to the difference in the failure mode and non-inclusion of anchorage length consideration in the strut-and-tie method.

4.2 Load-Deflection Response

The deflection at midspan corresponding to the applied load is presented in Figs 12, 13, and 14.

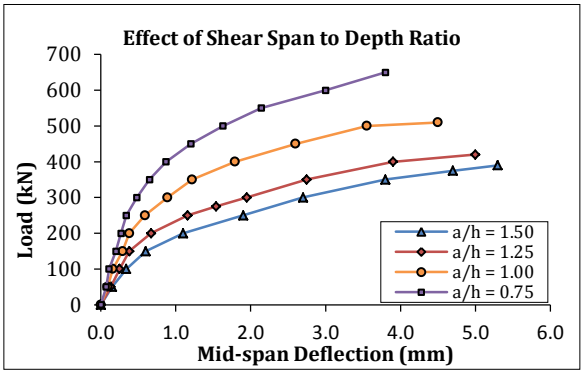

Figure 12. Load - Deflection Curves for specimens with a/h effect

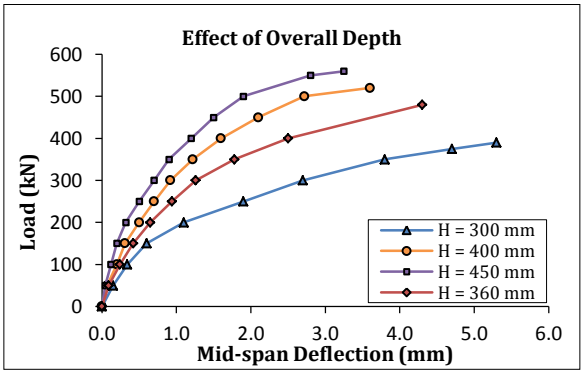

Figure 13. Load - Deflection Curves for specimens with H effect

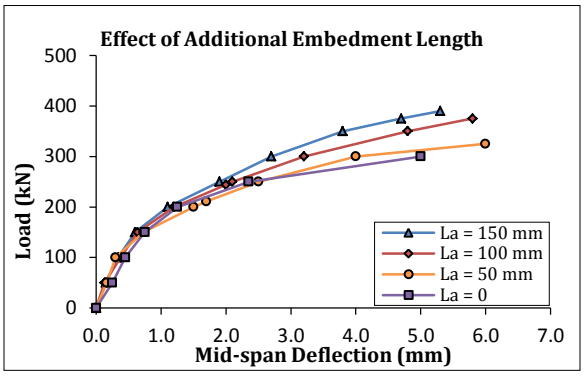

Figure 14. Load - Deflection Curves for specimens with la effect

The deflections at the service load stage were used to describe the actual behavior of beams under loading. For instance, when the applied load reached 65% of the failure load, which represents the applied service load as recommended by [21].

From Figs 12, 13, and 14 it is noted that for the specimens (Control Beam, DB2-La, and DB3-La) with development lengths = 150 mm, 100 mm, and 50 mm, the deflection at service load is increased by 62%, 67%, and 42% respectively compared with DB4-La with zero development length. For the specimen (DB2-H, DB3-H, and DB4-H) with depth = 360 mm, 400 mm, and 450 mm respectively, the deflection at service load is decreased by 33%, 38%, and 51% respectively compared with the control beam with an overall depth equal to 300 mm. For the specimens (DB2-a, DB3-a, and DB4-a) with a/h = 1.25, 1.00, and 0.75 the deflection at service load is decreased by 3%, 14%, and 62% respectively compared with the control beam with a/h = 1.5.

4.3 Cracks Propagations

The cracking propagation patterns at the failure of the tested beams are shown in Fig 15. Every crack is signified by a line that characterizes the crack's direction and length. Four deformation stages from the initial loading to the final ultimate load were noted: no visible crack, first flexural cracking, first diagonal cracking, and final failure. At the beginning of applying the loads, no cracks appear, and all specimens resist the loads without any visible deformation. The first flexural crack developed in the constant bending moment region at approximately (16-25)% of the ultimate loads. With additional load increase, the diagonal cracks suddenly formed close to the supports at approximately (33-50)% of the ultimate loads. After the formation of main cracks, the magnitude of the deflection increased rapidly which is associated with stiffness reduction. The crack propagation was influenced significantly by the (a/h) ratio, which for spec-

imens with larger (a/h) values recorded earlier development of hairline flexural cracks and diagonal cracks. The overall depth of the section has a pronounced effect on the development of the first crack, which for the beams with larger (h) showed slow development of hairline flexural cracks with less well-defined for the first diagonal crack. For the beams with the (la) effect, by decreasing the (la) the first hairline flexural cracking and diagonal cracking loads decrease as well.

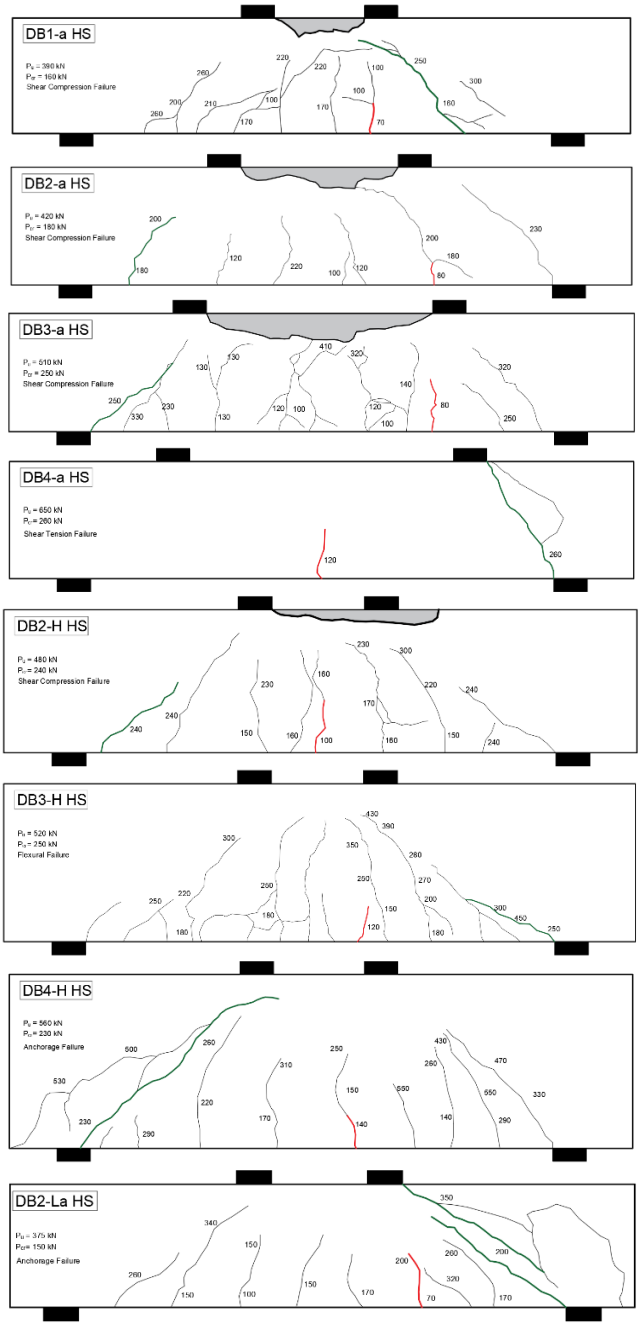

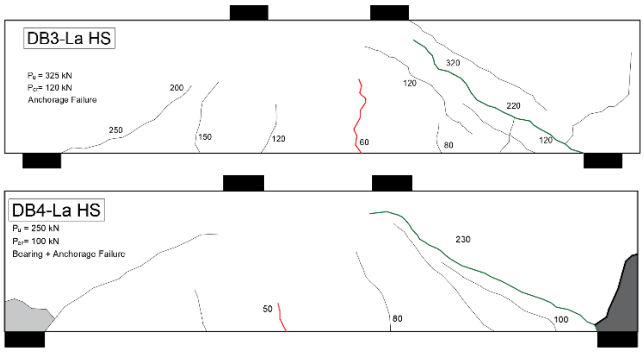

Figure 15. Crack Propagation Patterns at Failure.

4.4 Failure Mechanism

The failure mechanism of the tested deep beams is very important to investigate the anchorage details on the failure modes. Generally, It is observed that for the high strength concrete the tensile steel reinforcement has to yield prior to concrete crushing and lead to different failure modes. Five failure mechanisms are noted in this study.

- Shear-Compression Failure

This failure type takes place close to the points load of beams due to concrete crushing. The concrete reaches the ultimate load capacity after the yielding of the steel reinforcement and no-load distribution is possible. It was observed in beams [The control beam (DB1-a), DB2-a, DB3-a, and DB2-H].

- Shear-Tension Failure

This failure typically occurs when the bond between steel reinforcement bars and the surrounding concrete is reduced due to horizontal cracks. It was noted in beams (DB4-a) only, with a/d equal to 0.75.

- Flexure Failure

Flexural failure occurring due to the yield of the bottom reinforcement bars without concrete crushing of concrete at the loading points. This failure type was observed in beam DB3-H.

- Anchorage Failure

Anchorage failure takes place when the concrete cover splits out in the longitudinal direction associated with an inclined crack propagating from the support point to the point load direction. It was noted in deep beams with a shorter embedment length beyond the support and suitable bearing size (no bearing failure) as shown in beams DB4-H, DB2-la, and DB3-la.

- Bearing and Anchorage Failure

Bearing failure is the concrete crushing above the beam supports which takes place due to the small size of the bearing plate. This failure was observed in beams (DB4-La) and followed by anchorage failure.

5. Conclusions

In the current study, ten deep beams were cast and tested to investigate the shear capacity of high strength concrete deep beams with short straight anchorage length. The strut-and-tie method according to the ACI 318-14 was used to predict the deep beams capacity and failure modes. Three main parameters were considered which were the shear span to overall depth (a/h) ratio, the overall depth of section, and the additional embedment length beyond the support. Based on the results the following main conclusions are drawn upon:

1- The shear-span to the overall depth ratio is the critical parameter that controls the behavior and shear capacity of reinforced concrete deep beams. The decrease in the shear span to the overall depth ratio through values 1.5, 1.25, 1.0, and 0.75 leads to an increase of the ultimate capacity by 8%, 31%, and 67% respectively compared with the control beam. The increase in shear span to the overall depth ratio leads to a decrease in cracking loads and an increase of the midspan deflection at the service load. That attribute to increasing the arm of force (a) leads to an increase in the bending moment, and the increase in bending moment means an increase in deflection. This increase in inclined cracking and ultimate loads are due to the higher contribution of arch action shear transfer in beams with a lower a/d.

2- There is a pronounced effect of the overall depth on the shear capacity of the deep beam. An increase in the overall depth of the beam leads to an increase in the load-carrying capacity by 17%, 38%, and 55% respectively compared with the control beam. The first cracking load increases as overall depth increases and the midspan deflection at the service load decreases.

3- The end anchorage details are an important parameter that affects the beam behavior and shear capacity. The progressive reductions of the additional embedment length beyond the support for the straight anchorage detail yields to proportional reductions in the ultimate loads due to the reduction of the bond strength after nodal zones which caused the anchorage failure mostly.

4- Generally, for high concrete compressive strength specimens, the yielding of the tension reinforcement takes place and the compression strut crushing is occur.

5- Bearing failures were found associated with anchorage failure for the beams with short additional embedment length beyond the supports and influenced on the strengths.

6- The strut and tie model according to ACI 318-14 provides good agreement to predict the deep beam capacity compared with the experimental results.

6. Nomenclature

F_{ns} : The nominal compressive strength of a strut.

f_c' : Specified compressive strength of concrete, MPa.

f_{ce} : The strength coefficient.

β_s : Strut coefficient.

A_{cs} : The cross-sectional area at the end of the strut.

F_{ns} : The nominal compressive strength of a tie.

A_{ts} : The area of non-prestressed reinforcement in a tie, mm^2.

f_y : Specified yield strength of non-prestressing reinforcement, MPa.

F_{ns} : The nominal compressive strength of a nodal zone.

f_{ce} : The effective compressive strength of concrete at the face of a nodal zone.

A_{nz} : The smaller area of the face of the nodal zone is taken perpendicular to the line of action of the strut, tie, or applied load.

β_n : Nodal zone coefficient.

7. References

[1] Kamaran S. Ismail, Shear Behaviour of Reinforced Concrete Deep Beams, Ph.D. Thesis, Department of Civil and Structural Engineering, University of Sheffield, 2007.

[2] ACI Committee. Building Code Requirements for Structural Concrete (ACI 318-14) and Commen-

tary. American Concrete Institute, 2014.

[3] Kong, F. K., ed., Reinforced Concrete Deep Beams, Van Nostrand Reinhold, 1990, 288 pp.

[4] ACI Committee. Guide to Quality Control and Assurance of High-Strength Concrete (363.2R-11). American Concrete Institute, 2011.

[5] BouSaleh Ahmad, Effects of Anchorage Details on Response of Deep Beams, M.Sc. Thesis, Department of Civil Engineering and Applied Mechanics, University of McGill, Canada, 2006.

[6] Maruful H. Mazumder, The anchorage of deformed bars in reinforced concrete members subjected to bending, Ph.D. Thesis, School of Civil and Environmental Engineering, University of New South Wales, Australia (2014).

[7] Jaber M. Alsiwat and Murat Saatcioglu, Reinforcement Anchorage Slip under Monotonic Loading, Journal of Structural Engineering, Vol. 118, Issue 9, 1992

[8] Azizinamini, A. et al., Bond performance of reinforcing bars embedded in high-strength concrete, ACI Structural Journal, V. 90, pp. 554-561, 1993.

[9] Zhen Yu Li, Behaviour and Modeling of Deep Beams with Low Shear Span-to-Depth Ratios, M.Sc. Thesis, Department of Civil Engineering, and Applied Mechanics, University of McGill, Canada, 2003.

[10] Adebar, P. and Zhou, Z., Bearing strength of compressive struts confined by plain concrete, ACI Structural Journal, Vol. 90, pp. 534-541, 1993.

[11] Sung-Gul H. et al., Shear Strength of Reinforced Concrete Deep Beams with End Anchorage Failure, ACI Structural Journal, V. 99, No. 1, 2002.

[12] Fung-Kew K. et al., Effect of Embedment Length of Tension Reinforcement on the Behavior of Lightweight Concrete Deep Beams, ACI Structural Journal, V. 93, No. 1, 1996.

[13] ASTM C150/C150M. Standard Specification for Portland Cement. American Society for Testing and Material, 2015.

[14] ASTM C136/C136M. Standard Test Method for Sieve Analysis of Fine and Coarse Aggregates. American Society for Testing and Material, 2014.

[15] ASTM C33/C33M. Standard Specification for Concrete Aggregates. American Society for Testing and Material, 2013.

[16] ASTM C1602/C1602M. Standard Specification for Mixing Water Used in the Production of Hydraulic Cement Concrete. American Society for Testing and Material, 2012.

[17] ASTM C494/C494M. Standard Specification for Chemical Admixtures for Concrete. American Society for Testing and Material, 2015.

[18] ASTM C1017/C1017M. Standard Specification for Chemical Admixtures for Use in Producing Flowing Concrete. American Society for Testing and Material, 2013.

[19] ASTM A615/A615M. Standard Specification for Deformed and Plain Carbon-Steel Bars for Concrete Reinforcement. American Society for Testing and Material, 2015.

[20] ACI Committee. Specifications for Structural Concrete (ACI 301M-10). American Concrete Institute, 2010.

[21] Emadaldeen A., and Jamal A. Experimental Study on The Behavior and Strength of Reinforced Concrete Corbels Cast with Self-Compacting Concrete Incorporating Recycled Concrete as Coarse Aggregate. International Journal of Civil Engineering and Technology (IJCIET) Volume 10, Issue 1, January 2019, pp.188–201, Article ID: IJCIET_10_01_018.